NOAA Technical Memorandum ERL FSL-6

DEVELOPMENT AND TESTS OF A CLOUD PHYSICS PARAMETERIZATION FOR REAL-TIME AVIATION AND PUBLIC NUMERICAL WEATHER FORECASTING

Paul Schultz

Forecast Systems Laboratory
Boulder, Colorado
April 1993

noaa NATIONAL OCEANIC AND ATMOSPHERIC ADMINISTRATION / Environmental Research Laboratories

NOAA Technical Memorandum ERL FSL-6

DEVELOPMENT AND TESTS OF A CLOUD PHYSICS PARAMETERIZATION FOR REAL-TIME AVIATION AND PUBLIC NUMERICAL WEATHER FORECASTING

Paul Schultz

Forecast Systems Laboratory
Boulder, Colorado
April 1993

UNITED STATES
DEPARTMENT OF COMMERCE

NATIONAL OCEANIC AND
ATMOSPHERIC ADMINISTRATION

Environmental Research
Laboratories

NOTICE

Mention of a commercial company or product does not constitute an endorsement by the NOAA Environmental Research Laboratories. Use of information from this publication concerning proprietary products or the tests of such products for publicity or advertising is not authorized.

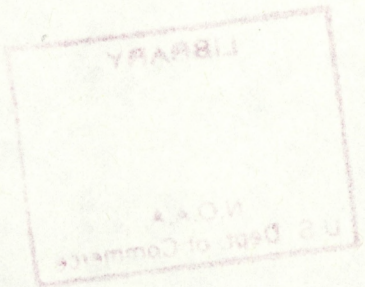

For sale by the National Technical Information Services
5285 Port Royal Road, Springfield, VA 22061

CONTENTS

TABLES

FIGURES

Development and Tests of a Cloud Physics Parameterization for Real-Time Aviation and Public Numerical Weather Forecasting

Paul Schultz

ABSTRACT. A package of FORTRAN subroutines for parameterizing condensation and precipitation processes in mesoscale models is described. The code is tailored to the requirements of operational weather forecasting for the aviation community and for public weather forecasting. As such, the emphasis is on computing efficiency, performance verification, simplicity of design (for rapid problem resolution), and regional tailorability.

Results from preliminary testing are presented. A variety of procedures illustrate model attributes such as water mass conservation and physical realism, and some of the algorithm's limitations.

The anticipated context for this effort is the moist-processes component of a mesoscale four-dimensional data assimilation system now under development at the NOAA Forecast Systems Laboratory for the Aviation Gridded Forecast System.

1. INTRODUCTION

This report describes the development of a cloud microphysics parameterization for use in updraft-resolving numerical weather forecasting models. The design considerations motivating this development are

- Three-way compatibility among operationally available observations, model variables, and forecasting service requirements.
- Regional and seasonal tailorability.
- Simplicity, specifically to enable straightforward problem detection and correction.
- A computing infrastructure compatible with massively parallel processing.

This effort is a part of the Aviation Gridded Forecast System (AGFS) development

by the NOAA Forecast Systems Laboratory (FSL) in Boulder, Colorado, under sponsorship of the Federal Aviation Administration (FAA). Appendix A describes FSL's local-scale modeling plan for AGFS.

The function of a cloud microphysics parameterization in a mesoscale model is to compute, at each gridpoint, the changes in phase, type, and quantity of condensate; and the production, fallout, and (mid-air) evaporation of precipitates. It is the task of the host mesoscale model to compute advection and latent heating, i.e., the related dynamical processes.

The first design consideration stated above is three-way compatibility among observations, model variables, and required model outputs. The intended ultimate application of this package is within a four-dimensional data assimilation (4DDA) system. One approach to 4DDA is known as "Newtonian nudging" (Stauffer and Seaman, 1990), in which 1) observations (e.g., satellite, radar, gauge) are used to produce objective gridded analyses of the condensate fields; 2) objective analyses are used to initialize the mesoscale model; 3) the model forecasts are used as first guesses to subsequent objective analyses; 4) the model is re-run with additional, nonphysical, forcing terms that "nudge" the model solution toward the analyzed state to produce an improved model initialization from which a better forecast should result; and 5) the cycle returns to step 2. At this date, many important pieces of such a system exist or are being developed at FSL. Most relevant among these is the Local Analysis and Prediction System (LAPS) three-dimensional cloud analysis package (Appendix B), which is the component that accepts observations and produces the gridded analyses of water condensate. The microphysical code described here is designed so that the cloud variables are defined as they will exist in the LAPS cloud analyses, to the extent possible.

The categories of condensate in this algorithm are cloud liquid c, cloud ice p (for "pristine crystals"), rain r, snow s, and ice i (which includes heavily-rimed snow, graupel, hail, and sleet). In some aspects of the parameterization, physical realism is sacrificed when the goals of the model are not compromised. For example, in nature, both cloud liquid

and cloud ice have nonzero fall velocities, but those fall velocities are assumed here to be zero, because they are very small and nothing is gained (for our purposes) by attempting to account for descending cloud matter. The practice of including only those physical processes that have important and known impacts on the forecast results was endorsed in the final report of the first international cloud modeling workshop sponsored by the World Meteorological Organization (WMO 1986, pp. 38–39).

To facilitate rapid problem diagnosis by future model users (e.g., Science Operations Officers at NWS forecast offices), the approach here is to preserve the simplicity of the code wherever possible, and to incorporate complexity only when the benefits of so doing are demonstrated. Attendant with the development of the microphysics parameterization is the development of advanced model forecast performance verification methods, which are the subject of a companion report forthcoming.

2. ALGORITHM DESCRIPTION

Figure 1 depicts the representation of cloud microphysical processes in this parameterization. The conservation equations are presented in Table 1. This section describes the important assumptions incorporated in the algorithm.

- All water vapor above saturation with respect to water is converted immediately to condensate.

- Vapor condenses into cloud liquid only. Production of cloud ice is represented as condensation into cloud liquid and subsequent freezing. Cloud liquid freezes into cloud ice, and cloud ice melts into cloud liquid. The Bergeron process of ice particle growth (i.e., that caused by the lower saturation vapor pressure over ice compared to that over liquid) is neglected[1]; however, the retarded evaporation of ice particles

[1] At $-12°C$, the temperature at which this effect is largest, the difference in saturation vapor pressure over ice compared to liquid results in a maximum of 0.17 g/kg of frozen condensate not produced at 1000 mb. This amount increases linearly to 0.34 g/kg at 500 mb. At any pressure elevation, this is 12.4% of the total vapor content.

by this processes is included (next bullet).

- If the grid point is subsaturated, cloud liquid and cloud ice are assumed to evaporate instantaneously until saturation or complete removal. Rain, snow, and ice evaporate at rates proportional to the vapor deficit. The computed vapor deficits over pristine crystals, snow, and ice are with respect to ice saturation; thus a descending parcel containing snow and rain will lose all its rain before any of its snow.
- Cloud liquid and cloud ice have zero fall velocity.
- Rain freezes reversibly into precipitating ice; snow melts into rain irreversibly.
- Rain does not grow by diffusional growth. Rogers and Yau (1989, Ch. 7) show that this process is negligibly slow.
- Diffusional growth of snow is artificially represented as production of cloud ice and subsequent conversion to snow.
- Only snow collects cloud ice.
- A three-way competition for cloud liquid by rain, snow, and ice is resolved by calculating the amounts each species would collect as if each were alone with cloud water in the grid box, then parsing an amount of available cloud liquid among the competing species, prorated according to their respective calculated affinities.

3. CONVERSION FUNCTIONS

The functions that compute the conversion rates between the condensate categories are extremely simple. Each is designed so that a single scalar "tuning knob" controls the magnitude of the function. The rate control parameters can then be read into the model from external tables. This is the mechanism for providing regional or seasonal tailorability.

First guesses for the settings of the conversion rate parameters (tuning knobs) were based on intuition only. For example, the rate control parameter for the evaporation of rain is set to $8.33 \times 10^{-6}\ kg/kg/s$, which corresponds to $1\ g/kg$ of rain evaporating completely

in 2 min. This estimate is based loosely on the author's observations of evaporating virga shafts extending from high-based thunderstorms. One important aspect of this model development approach is that the rate control parameters will be adjusted using an objective, empirical optimization technique, discussed briefly in the Conclusion.

The conservation equations for this model are given in Table 2. The conversion functions are shown in Figure 2, and given in equation form in Table 3.

Some of these processes are independent of the presence of other gases; for example, collections are the result of physical proximity among particles. For these, the amounts of condensate are expressed as specific contents q_x, (kg_x/m^3). Others are affected by the other gases; for example, freezing and melting occur faster in a relatively dense medium, because heat exchange is accomplished by molecular interactions between particles and the gases surrounding them. For these, the amounts of condensate are expressed as mixing ratios r_x, (kg_x/kg_{air}). The conversion factor between the two expressions is the density of air ρ (kg_{air}/m^3), or its reciprocal. For practical purposes, it is convenient that $\rho \approx 1$ in MKS units.

Since cloud liquid and cloud ice freeze and melt into each other, this pair of processes is represented as a single reversible ("two-way") process. Likewise, the freezing of rain and the melting of precipitating ice are represented as a single reversible process.

Supercooled cloud liquid (Fig. 2a) is quite durable in the temperature range between -5°C and 0°C, where the conversion rate is set to zero. Below -5°C the conversion function is quadratic down to -20°C, where the maximum freezing rate is reached. Pristine crystals melt very quickly above freezing.

All collection processes are based on the assumption that the rate depends on the specific contents of both the collected and collecting species. These four conversion functions have similar forms. Following Kessler (1969), a minimum amount of the collected species (0.5 g/m^3 at this time) must be present before collection begins. Autoconversion is included implicitly in the warm rain function (Fig. 2d) and the snow generation function

(Fig. 2g). Note the nonzero conversion rates in these two figures when the collector amounts are zero.

In many of these functions, limits are imposed on the maximum conversion rates. These are to minimize model shock in the event that other influences in the model (e.g., numerical noise from advection) produce spurious condensate amounts that might cause subsequent spurious microphysical conversions.

4. TESTS

A variety of simple tests were conducted to expose any flaws in the design and code, and to demonstrate basic software integrity. In the process, some problems in the original structure of the algorithm "flow" were identified, which required a nearly complete rewrite of the main module. Other tests suggested simple but gross changes in the conversion functions and tuning knobs. The results to follow are a small subset of the entire testing effort.

At this stage, the attributes being evaluated are physical plausibility, numerical stability, and water mass conservation. Future efforts will concentrate on optimizing agreement with observations, i.e., from field experiments, and evaluating candidate improvements to the conversion functions.

a. Lagrangian parcel tracks. Figure 3 shows the condensate amounts in a parcel as it is carried aloft by a thunderstorm updraft, as a function of height (Fig. 3a) and of time (Fig. 3b).

Profiles of temperature and vertical velocity are specified; there is no latent-heating buoyancy forcing. The parcel moves along a moist adiabat with characteristic equivalent potential temperature $\theta_e = 280K$. The initial parcel attributes are $T = 5°C$, $p = 950\ hPa$, $RH = 95\%$. The vertical velocity profile is parabolic in height, with $w_{max} = 10\ m/s$ and $w = 0$ just below the initial parcel height (500 m) and at cloud top (10000 m).

The results show cloud liquid formation until about 0.5 g/kg, and rain formation

shortly thereafter. Graupel (ice) begins to form when rain is carried by the updraft above the freezing level (1300 m, 855 mb). Not long after cloud liquid begins to freeze into pristine crystals, the crystals begin to aggregate into snow. Since snow, rain, and graupel all collect cloud liquid, the cloud liquid is almost completely depleted at 4000 m, where all three are present.

Note that the mixing ratio of cloud ice increases (slowly) with altitude, which is consistent with the discussion of Kessler (1969, p. 14). This is because the scavenging of cloud ice by snow is retarded by increasing distance between particles in the less-dense medium. The specific content of cloud ice (not shown) remains relatively constant.

Three problems are evident in this simulation. First, snow content aloft is greater than the original available vapor content. This traces to the formulation for condensate fallout used here. The condensate tendency resulting from settling is the difference between the amount that fell in from above and the amount that fell out. For this test, that process was calculated as the difference between the estimated fallout at successive time steps, assuming the current amount is a reasonable guess for what fell in, and the past amount is a reasonable guess for what fell out. This is obviously nonconservative, but not necessarily nonphysical, because parcels can gain condensate mass in this manner. However, snow mixing ratios over 7 g/kg are nonphysical. The problems caused by this representation of fallout are not serious because the settling calculation is much more straightforward in the destined Eulerian (gridded) framework.

The second problem is a numerical glitch that appears at the end of the ice (graupel) time series, which is also the result of the fallout calculation.

The third problem is that the cloud liquid is completely depleted too soon. This is the sort of problem that should be addressed by tuning the conversion rates, but that is for future work.

Figure 4 shows the condensate amounts in a parcel as it descends slowly (1 m/s), as a function of height (Fig. 4a) and of time (Fig. 4b). This is not a realistic meteorological

situation, but it illustrates the melting and evaporation processes in the model. Condensate settling is turned off. The initial parcel attributes are $T = -9°C$, $p = 500\ hPa$, $z = 5500\ m$, $r_v = r_{satliq} = 3.97\ g/kg$, $r_c = 0.6\ g/kg$, $r_r = 1\ g/kg$, $r_p = 0.6\ g/kg$, $r_s = 1\ g/kg$, $r_i = 1\ g/kg$. The parcel descends along a moist adiabat at $-1\ m/s$.

The evaporation treatment in the model reflects two facts: small particles evaporate before large particles, and liquid evaporates before ice (due to the lower saturation vapor pressure over ice compared to liquid). Although the model does allow some freezing of cloud liquid at the initial parcel temperature ($-9°C$), it is quite slow, and evaporation consumes all the cloud liquid almost immediately. The rain begins to evaporate, but not fast enough to keep the parcel saturated; in fact, the parcel's vapor pressure falls below even the saturation value over ice. Thus, the pristine crystals begin to evaporate by 600 s, and by 1000 s are completely gone. Later, the snow and precipitating ice (graupel) begin to melt into rain, the snow faster than the ice. The last of the rain has evaporated by the time the parcel has lowered to 2230 m.

In the textual model output (not shown), the mixing ratios are presented to five digits of precision. The sum of vapor and condensate at the beginning of the simulation was 8.0768 g/kg; the amount of vapor at the end of the simulation (after all the condensate had evaporated) was identical. The conversion processes exercised in this test conserved water mass within the available precision.

b. 1-meter slab. A quasi-two-dimensional dynamical framework similar to a strong stationary thunderstorm updraft was used to test the conservation properties of all the conversion processes in gridded context. The grid has a 1-km horizontal grid increment and a 200-m vertical grid. The grid is 61 $\times$ 51, so the domain is 60 km $\times$ 10 km.

The initial conditions are shown in Figure 5. The wind field (Fig. 5a) is a pair of solenoids acting to produce a single updraft. There is no wind component normal to the boundaries, so there is no transport of mass, momentum, heat, or moisture into or out of the domain. The maximum horizontal wind speed is 20 m/s; the maximum vertical velocity is about 9 m/s. The sounding is shown in Figure 5b. The temperature, pressure,

and wind fields are invariant; there is no latent heating.

The moisture fields after 30 min are shown in Figure 6. The deformation on the moisture field produces dry advection from above on the sides and a moist plume in the middle. A substantial rain water field has developed; in fact, 45 mm have already fallen. An unrealistically large amount of rain water remains suspended (max = 17 g/kg), because the updraft, whose maximum speed is greater than rain's maximum fall velocity, is unrealistically long-lived, at least for a single updraft. The anvil at cloud top is mostly cloud ice, although a large amount of snow (3 g/kg) exists immediately above the strongest updraft.

After 30 min, the wind field was reversed to force melting and evaporation (not shown). This is not a meteorologically plausible scenario, but the intent of this exercise is to apply all the conversions included in the model. After 60 min, by which time the microphysical model has been called several hundred thousand times, the total water mass change is -642 kg out of a total of 3.25 million kg in the domain, or -0.02%. This represents sufficient water mass conservation for all anticipated purposes.

c. Lagrangian column. This test illustrates the simulated evolution of a column of air embedded in steady upslope flow.

The initial parcel sounding is a slightly sub-saturated moist adiabat ($\theta_e = 280K$). At each of the 20 levels in the vertical ($\delta z = 200$ m), the parcel pressure was reduced 1 mb at each 30-s time step. The implied vertical velocity is about 0.33 m/s, which roughly approximates the vertical motion associated with 5 m/s easterly (upslope) flow from Boulder ($z = 1600$ m) to the Continental Divide ($z = 3600$ m) 30 km to the west, in 100 min. As before, there is no latent heating feedback to the airflow.

The results are shown in Figure 7. The cloud matter distribution is shown in Figure 7a. In Figures 7b, 7c, and 7d showing rain, snow, and ice, respectively, the top diagram shows the results of this simulation with no fallout; i.e., any produced condensate was carried along by the parcel. The bottom diagram shows the surface precipitation from

the same simulation with fallout included. Very little precipitation is suspended in the latter case, since the vertical velocity, which is constant throughout the column for the entire duration, is small compared to the particle fall velocities. The cloud matter shown in Figure 7a is from the simulation with fallout included.

Within the first 15 min, or about 5 km up the hill, a thick, all-liquid cloud forms (Fig. 7a). From that point on, the cloud top begins to glaciate. A large gradient in the concentrations of both cloud liquid and cloud ice is evident near the $-9°C$ $(264K)$ isotherm.

At the same time (by chance), rain begins to fall (Fig. 7b). In fact, rain is the only precipitation type for the next 15 min of the column's track, forming a band about 5 km wide. To be precise, since the maximum precipitation rate is less than 2 mm/h, this should be considered drizzle.

About one-half hour into the simulation, a burst of precipitating ice appears, followed by a more steady production for the rest of the period. In the author's *in-situ* observations of steady upslope conditions, the transition from drizzle to snow is sometimes accompanied by a burst of very heavily rimed fast-falling ice particles, followed by steadier precipitation. More often than not, these events are probably caused by weak convection, although this test suggests a possible different mechanism, because there are no convective processes involved in this run. The production mechanisms for the precipitating ice category are freezing drizzle, heavily-rimed snow, and rimed ice particles. In this simulation, the rainmaking process left behind enough cloud water to be scavenged by what small amounts of ice and snow were being generated, and shortly after that, the three precipitating species effectively used up the available cloud water, down to its set minimum value $(0.5\ g/kg)$.

Figure 7a illustrates a persistent problem in modeling moisture processes in the atmosphere. Even with perfectly smooth kinematic forcing, the resultant fields of condensate are not similarly smooth. Note that the high-gradient zone near the $264K$ isotherm is not very smooth. In fact, earlier, rougher-looking versions of this simulation motivated

the smoother cloud-matter freezing function shown in Figure 2a. If there were latent-heating feedback into the model, this would probably produce some sort of high-frequency shock response. This shock may be physically realistic, because sudden latent heat release can cause gravity waves, for example, in the case of large deep convection. However, it may also cause non physical numerical problems. Ooyama (1990) concludes that since "the numerical problem associated with the phase changes of water substance is rooted in thermodynamics . . . the problem should be solved within thermodynamics [parameterizations]." Ooyama proposes, for example, a hyperbolic tangent function through $0°C$, instead of the physically correct step function, to describe latent heat release. This problem is noted here to call attention to this candidate source of model noise, and to suggest that solutions to the problem, should it arise in future applications of the present algorithm, might be approached by using smoothed conversion functions if they produce better results than those based on theoretical principles or laboratory results.

5. CONCLUSION

The next steps in the development of this algorithm are to 1) implement it as a microphysics option of the Colorado State University Regional Atmospheric Modeling System, CSU-RAMS; 2) run the model with identical initial conditions as those used in published simulations; 3) permute the microphysical conversion rate parameters; and 4) determine the optimum settings for those parameters according to objective verification statistics. Lee (1992) used the Multiple-Response Block Permutation (MRBP, Mielke 1991) agreement measure to evaluate the relative success of experimental model runs in a similar application involving 13 processes in a parameterization of vegetated-surface fluxes of heat, momentum, and moisture.

The chosen test cases will be quasi-two-dimensional meteorological scenarios, such as an upslope snowstorm and a propagating convective squall line, because cross-section versions of the model run many times faster than full three-dimensional runs. That will be important in the model tuning process, because the model must run in its entirety for each permutation of the conversion rate parameter settings, requiring many model runs.

Of course, the quality of a model is ultimately established by verification against real data, not simulations. The parameter settings arrived at during the tuning process can serve as defaults in a real-time 4DDA system. *In-situ* observations of cloud microphysical attributes are available only for relatively few cases from field projects, but precipitation type and intensity are always available, in real time, via LAPS. Because precipitation is the integrated result of microphysical processes aloft, model agreement with observed precipitation, in the context of 4DDA as described in the Introduction, is an appropriate goal.

Appendix A – Local-scale modeling at FSL

The NOAA Forecast Systems Laboratory is conducting mesoscale 4DDA system development in support of the Aviation Gridded Forecast System project sponsored by the Federal Aviation Administration. This project is aimed at exploiting rapid concurrent technological advances in weather observations systems, data assimilation procedures, digital computing, telecommunications, and computer workstations to provide weather services in support of the national aviation community. The 4DDA system is designed to incorporate all the available data sets for the purpose of providing aviation weather services of the greatest possible accuracy and detail.

Contemporary operational weather forecasting models parameterize the effects of all convection. However, several research models exist that are capable of explictly resolving and simulating individual (large) thunderstorms with impressive success. This requires much finer grid spacing than is found in current operational models, and different modeling procedures.

The National Meteorological Center's current plans for the coming decade are to produce centralized gridded analyses every hour, and to run a forecast model at 5-km grid resolution four times per day. This represents a significant improvement in grid resolution for operational modeling, but still underexploits the operational datasets. Given the vastly increased capabilities of emerging computing architectures, and the exclusive local availability of very high-resolution data sets, our goal is as follows:

Using the gridded model outputs from NMC as first guesses and boundary conditions, local analyses can be updated at 1-km horizontal resolution and at least 100-m vertical resolution every 5 min. Every hour, a model capable of explicit simulation of moist convection can be started 1 hour in the past and integrated forward, assimilating the 5-min analyses for the first hour of model run time, and forecasting out to 3 or 6 hours. During the forecast portion of the model run, the NMC grids provide the boundary conditions, and intermediate model outputs are saved to provide first guesses for subsequent 5-min analyses.

Our first implementation of a prototype AGFS, scheduled for July 1994, represents the first steps toward this goal.

On the national scale, the assimilation function will be provided by FSL's Mesoscale Analysis and Prediction System (MAPS). As of this date, MAPS is running on a 60-km horizontal grid covering the CONUS, but the plan is to increase the grid resolution to 15 km. MAPS ingests all the established data streams, such as surface observations and rawinsonde data, and many from the emerging new data sources, such as wind profilers and automated temperature and wind sensors aboard commercial aircraft. MAPS will produce hourly full-volume analyses. MAPS also has a short-range forecast component that provides first guesses for subsequent analyses.

The forecast function on the national scale will be provided by the Eta model being developed by NMC to replace the Nested-Grid Model as the operational guidance for NWS operations. FSL is working in close cooperation with NMC on development of the Eta Model. For FSL's implementation (and perhaps NMC's as well, eventually), the model will be initialized by MAPS analyses on 15-km horizontal grid mesh similar to that of MAPS.

On the regional scale, the data assimilation function will be accomplished by LAPS. LAPS is fully nested within MAPS, which provides first-guess fields to LAPS for subsequent refinement on a finer grid. Currently, LAPS analyses are on a 10-km grid covering a 600-km square centered on Denver. The eventual goal is to produce analyses on a 1- or 2-km grid. LAPS incorporates data from a surface mesonet, multiple Doppler radars, GOES satellite radiance data, and other sources, to refine the MAPS analyses. AThree-dimensional analyses of cloud cover and type and radar reflectivity are also provided.

The regional scale model will be CSU-RAMS, developed by the CSU Department of Atmospheric Science. It will be initialized by LAPS, and the boundary conditions during the forward integration are to be provided by MAPS. RAMS is a highly flexible numerical model that has been successfully applied to the study of hurricanes, synoptic-scale weather systems, convective storms, mountain-valley circulations, and turbulent eddies within the

planetary boundary layer. Ultimately, the model forecasts and LAPS analyses will merge to form a 4DDA package by nudging to LAPS analyses in the spin-up phase, and creating first guess fields for subsequent LAPS analyses in the forecast phase.

Appendix B – The LAPS Cloud Analysis

The cloud analysis package is a component of LAPS (McGinley et al. 1991), which is designed to use all operationally available datasets to produce three-dimensional grids of atmospheric attributes on a grid mesh compatible with the spatial density of the data. At this date, computer resource limitations and other practical considerations lead to a domain of 61 $\times$ 61 gridpoints, (10-km horizontal grid increment), a 1-h update cycle, and 21 pressure levels in the vertical (50-mb increment). However, the cloud analysis is generated on 42 height surfaces (100 m at the lowest level, 1000 m at highest level).

The steps in the analysis are

- "Soundings" of cloud coverage from SAOs and pilots' voice reports are distributed horizontally to produce a first-guess three-dimensional analysis.
- Satellite infrared cloud-top temperatures are converted to cloud-top heights using the temperature analysis. This information refines the horizontal distribution of clouds and the vertical limits of the cloud field.
- Three-dimensional radar data further refine the location and amount of cloud coverage.
- During the daytime, visible satellite data are used to reduce the coverage of thin clouds and sub-grid-scale scattered clouds.

Cloud coverage in percent is estimated at each point in the domain. Cloud type (e.g., Cu, St, Ci) is specified as a function of ambient temperature and the vertical gradient of equivalent potential temperature, $\frac{\partial \theta_e}{\partial z}$. Cloud type is determined at each gridpoint where the cloud cover fraction exceeds 0.65.

Vertical velocity within the clouds is estimated on the basis of cloud type and vertical extent. Constant values (currently 5 cm/s) are assigned for stratiform clouds; parabolic profiles are used in cumuliform clouds. This procedure does not assign vertical velocity estimates in cloud-free areas. The vertical motion estimates are used in the varia-

tionally balanced three-dimensional wind fields. It is expected that vertical velocity fields compatible with hydrometeor concentrations will be critical in successfully initializing the mesoscale model with diabatic processes in progress.

Cloud liquid and ice content are estimated using an adaptation of the Smith-Feddes technique, which was originally developed for use with rawinsonde data (McGinley and Albers 1991). In this application, the technique is used on each LAPS grid column as a sounding. The procedure assumes a parcel at cloud base is lifted to cloud top, calculates a maximum possible cloud liquid water content profile, and then makes adjustments based on assumptions of depletion by freezing. Further depletion is calculated where radar reflectivity data indicate the presence of precipitation-sized particles.

At this point, analyzed concentrations of rain, snow, and ice are not yet being produced, but the planning process is well under way. These will be generated using some combination of radar reflectivity, gauge data, and vertical profile assumptions.

REFERENCES

Kessler, E., 1969: On the distribution and continuity of water substance in atmospheric circulations. *Meteor. Monogr.,* **10,** #32, Amer. Meteor. Soc., 84 pp.

Lee, T.J., 1992: The impact of vegetation on the atmospheric boundary layer and convective storms. *Atmospheric Science Paper #509,* Colorado State University, 137 pp.

McGinley, J.A. and S.C. Albers, 1991: Validation of liquid cloud water forecasts from the Smith-Feddes method derived from soundings and LAPS analyses. *Preprints, 4th Int'l Conf. on the Aviation Weather System,* Paris, 24-26 June, Amer. Meteor. Soc., 228–233.

McGinley, J.A., S.C. Albers, and P.A. Stamus, 1991: Validation of a composite convective index as defined by a real-time local analysis system. *Wea. Forecasting,* **6,** 337–356.

Mielke, P.W., 1991: The application of multivariate permutation methods based on distance functions in the earth sciences. *Earth-Sci. Rev.,* **31,** 55–71.

Ooyama, K.V., 1990: A thermodynamic foundation for modeling the moist atmosphere. *J. Atmos. Sci.,* **47,** 2580–2593.

Rogers, R.R., and M.K. Yau, 1989: A Short Course in Cloud Physics. Third edition, Pergamon Press, 293 pp.

Stauffer, D.R., and N.L. Seaman, 1990: Use of four-dimensional data assimilation in a limited-area mesoscale model. Part I: experiments with synoptic-scale data. *Mon. Wea. Rev.,* **118,** 1250–1277.

WMO (World Meteorological Organization), 1986: Report of the international cloud modelling workshop/conference (Irsee, Federal Republic of Germany, 15–19 July 1985). WMO technical document WMO/TD-No. 139, Geneva, 460 pp.

Table 1 – Conservation equations

The terms in these equations are r for mixing ratios and C for conversion processes. The subscripts are v = vapor, c = cloud liquid, p (for pristine) = cloud ice, r = rain, s = snow, and i = precipitating ice. The coefficient α is a fraction between 0 and 1. Vt_r, Vt_s, and Vt_i refer to the fall velocities of rain, snow, and ice, respectively.

$$\frac{\partial(\rho r_v)}{\partial t} = -\vec{U} \cdot \nabla_3(\rho r_v) \pm C_{c\to v} + C_{p\to v} + C_{r\to v} + C_{s\to v} + C_{i\to v} \tag{1}$$

$$\frac{\partial(\rho r_c)}{\partial t} = -\vec{U} \cdot \nabla_3(\rho r_c) \mp C_{c\to v} \mp C_{c\to p} - C_{c\to r} - C_{c\to s} - C_{c\to i} \tag{2}$$

$$\frac{\partial(\rho r_p)}{\partial t} = -\vec{U} \cdot \nabla_3(\rho r_p) - C_{p\to v} \pm C_{c\to p} - C_{p\to s} \tag{3}$$

$$\frac{\partial(\rho r_r)}{\partial t} = -\vec{V} \cdot \nabla_H(\rho r_r) - (w - Vt_r)\frac{\partial(\rho r_r)}{\partial z} - C_{r\to v} + C_{s\to r} \mp C_{r\to i} + C_{c\to r} \tag{4}$$

$$\frac{\partial(\rho r_s)}{\partial t} = -\vec{V} \cdot \nabla_H(\rho r_s) - (w - Vt_s)\frac{\partial(\rho r_s)}{\partial z} - C_{s\to v} - C_{s\to r} + C_{p\to s} + \alpha C_{c\to s} \tag{5}$$

$$\frac{\partial(\rho r_i)}{\partial t} = -\vec{V} \cdot \nabla_H(\rho r_i) - (w - Vt_i)\frac{\partial(\rho r_i)}{\partial z} - C_{i\to v} \pm C_{r\to i} + (1-\alpha)C_{c\to s} + C_{c\to i} \tag{6}$$

Table 2 – Conversion processes

Although many other conversions among the five water species occur in nature (e.g., condensational growth of rain), these are the considered relevant to the present forecasting problems. These should suffice for capturing latent heating, precipitation, and clouds.

Vapor	advection condensation (−) evaporation of any condensate (+)	(1)
Cloud liquid	advection condensation (+) evaporation (−) melting cloud ice/freezing (+/−) accretion by rain (*collision/coalescence*) (−) accretion by snow or ice (*riming*) (−)	(2)
Cloud ice	advection evaporation (−) freezing cloud liquid/melting (+/−) aggregation to snow (−)	(3)
Rain	advection fallout (+/−) evaporation (−) freezing (−) melting snow or ice (+) accretion of cloud liquid (+)	(4)
Snow	advection fallout (+/−) evaporation (−) melting (−) accretion of cloud liquid (+) aggregation of cloud ice (+)	(5)
Ice	advection fallout (+/−) evaporation (−) melting (−) freezing rain (+) accretion of cloud liquid (+) conversion of rimed snow (+)	(6)

Table 3 – Conversion functions

The temperatures given below are in Kelvins if subscripted; degrees Celsius otherwise. The *maxrate* in each equation is the conversion rate parameter, or "tuning knob." For the collection functions ($C_{c\to r}$, $C_{c\to s}$, $C_{c\to i}$, and $C_{p\to s}$), the moisture variables are expressed as particle densities q_x, and the conversion rates have units of $kg_x/m^3/s$. For the others, the moisture variables are expressed as mixing ratios r_x, and the conversion rates have units of $kg_x/kg_{air}/s$.

$$C_{c\to p} = \begin{cases} maxrate, & \text{if } T < -20°C \\ maxrate \times \left(\frac{267 - T_K}{267 - 253}\right)^2, & \text{if } -20° < T < -6°C \\ 0, & \text{if } -6° < T < 0°C \\ -maxrate \times \left(\frac{T_K - 273.15}{278 - 273.15}\right), & \text{if } 0° < T < 5°C \\ -maxrate, & \text{if } T > 5°C \end{cases}$$

$$C_{c\to r} = \begin{cases} 0, & \text{if } q_c < q_{cmin} \\ maxrate \times \left(\frac{q_c - q_{cmin}}{.0015 - q_{cmin}}\right) \times \left(1 + \frac{q_r}{.002}\right), & \text{if } q_{cmin} < q_c < .0015 \\ maxrate \times \left(1 + \frac{q_r}{.002}\right), & \text{if } q_c > .0015 \end{cases}$$

$$C_{c\to s} = \begin{cases} 0, & \text{if } q_c < q_{cmin} \\ maxrate \times \left(\frac{q_c - q_{cmin}}{.0015 - q_{cmin}}\right) \times \left(1 + \frac{q_s}{.002}\right), & \text{if } q_{cmin} < .q_c < .0015 \\ maxrate \times \left(1 + \frac{q_s}{.002}\right), & \text{if } q_c > .0015 \end{cases}$$

$$C_{c\to i} = \begin{cases} 0, & \text{if } q_c < q_{cmin} \\ maxrate \times \left(\frac{q_c - q_{cmin}}{.0015 - q_{cmin}}\right) \times \left(1 + \frac{q_i}{.002}\right), & \text{if } q_{cmin} < q_c < .0015 \\ maxrate \times \left(1 + \frac{q_i}{.002}\right), & \text{if } q_c > .0015 \end{cases}$$

$$C_{p\to s} = \begin{cases} 0, & \text{if } q_p < q_{p_{min}} \\ maxrate \times \left(\frac{q_p - q_{p_{min}}}{.0015 - q_{p_{min}}}\right) \times \left(1 + \frac{q_s}{.002}\right), & \text{if } q_{p_{min}} < q_p < .0015 \\ maxrate \times \left(1 + \frac{q_s}{.002}\right), & \text{if } q_p > .0015 \end{cases}$$

$$C_{r\to v} = \begin{cases} 0, & \text{if } r_v > r_{satliq} \\ maxrate \times \left(\frac{r_{satliq} - r_v}{r_{satliq}}\right), & \text{if } r_v < r_{satliq} \end{cases}$$

$$C_{s\to v} = \begin{cases} 0, & \text{if } r_v > r_{satice} \\ maxrate \times \left(\frac{r_{satice} - r_v}{r_{satice}}\right), & \text{if } r_v < r_{satice} \end{cases}$$

$$C_{i\to v} = \begin{cases} 0, & \text{if } r_v > r_{satice} \\ maxrate \times \left(\frac{r_{satice} - r_v}{r_{satice}}\right), & \text{if } r_v < r_{satice} \end{cases}$$

$$C_{s\to r} = \begin{cases} 0, & \text{if } T > 0° \\ maxrate \times \left(\frac{T_K - 273.15}{283 - 273.15}\right), & \text{if } 0° < T < 10°C \\ maxrate, & \text{if } T > 10°C \end{cases}$$

$$C_{r\to i} = \begin{cases} maxrate, & \text{if } T < -20°C \\ maxrate \times \left(\frac{267 - T_K}{267 - 253}\right)^2, & \text{if } -20° < T < -6°C \\ 0, & \text{if } -6° < T < 0°C \\ -maxrate \times \left(\frac{T_K - 273.15}{278 - 273.15}\right), & \text{if } 0° < T < 5°C \\ -maxrate, & \text{if } T > 5°C \end{cases}$$

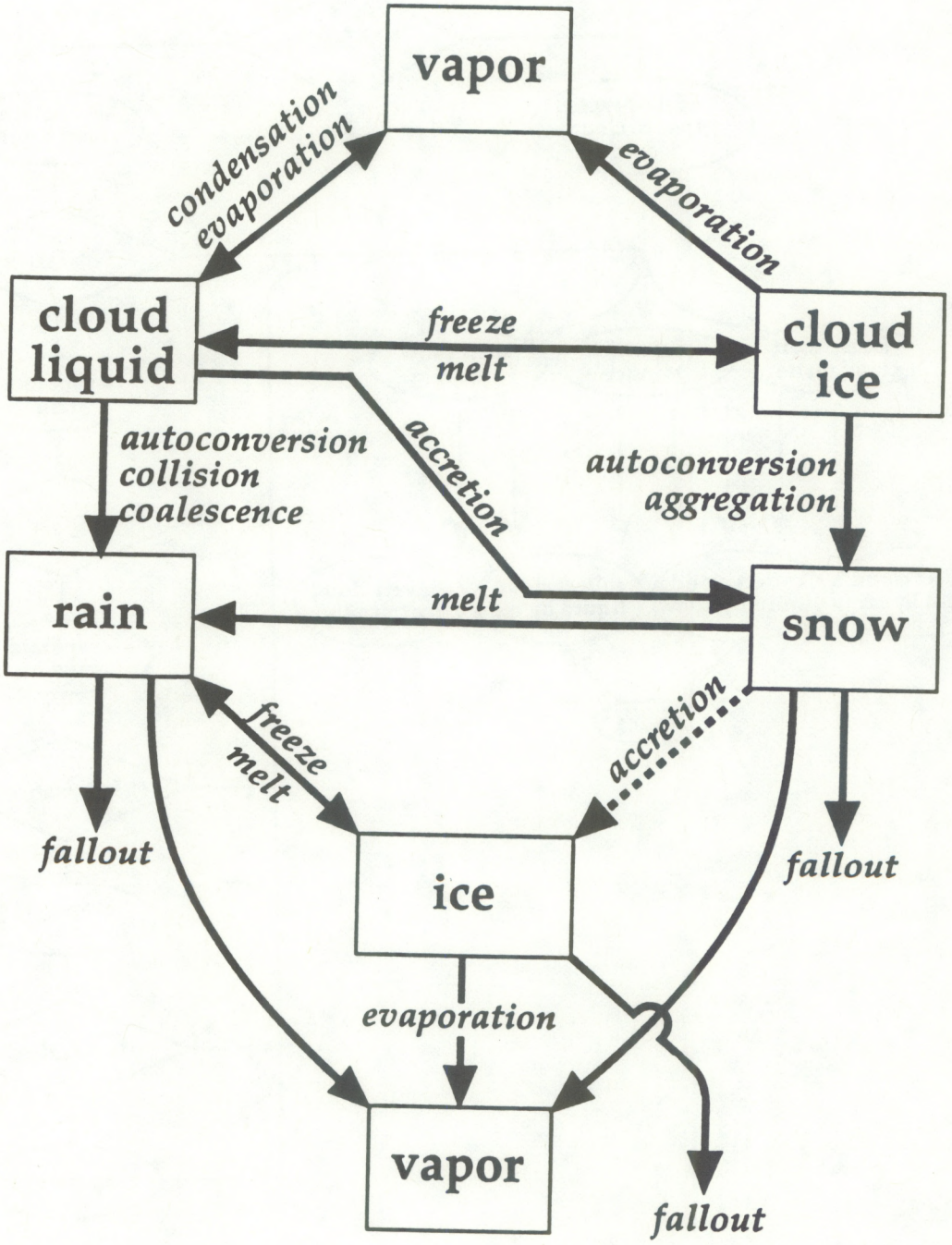

Figure 1a. Condensate categories (boxes) and conversion processes in the model. One-way and two-way processes are indicated by arrows. The dash arrow labeled "accretion" indicates that some of the rimed snow converts to graupel (ice).

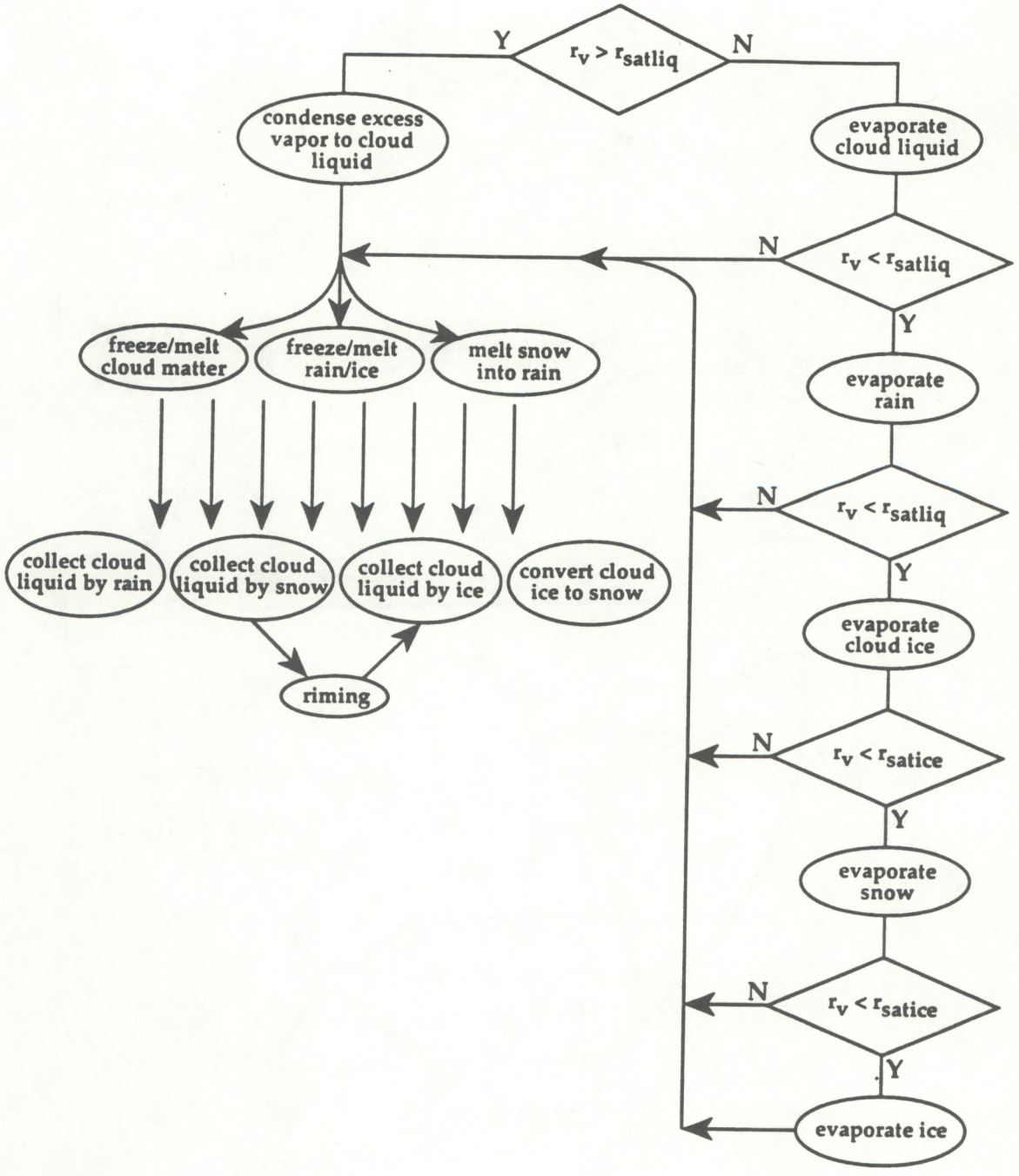

Figure 1b. Flow diagram of the microphysical algorithm.

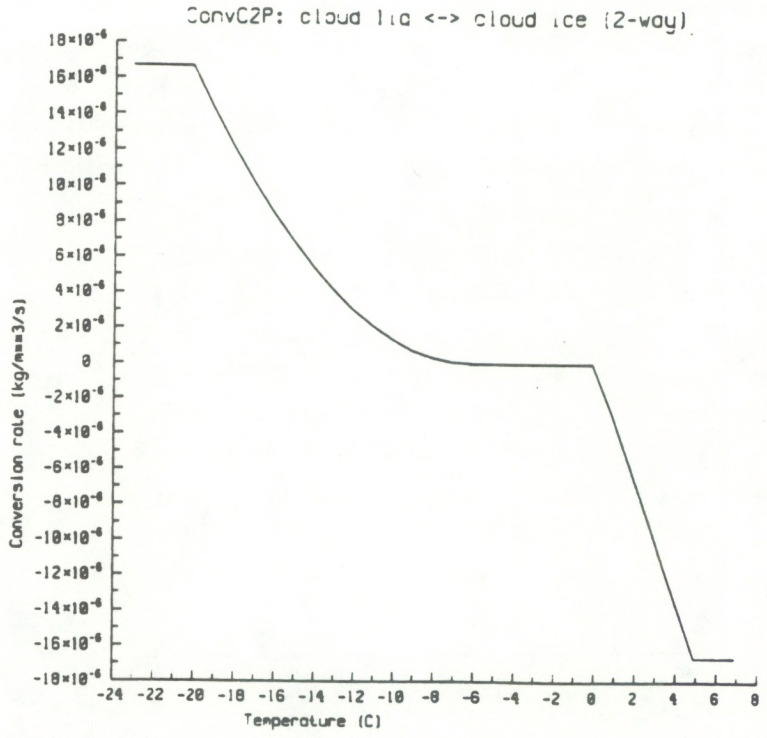

Figure 2a. Conversion function for cloud liquid freezing to cloud ice, and cloud ice melting into cloud liquid. The conversion rate parameter (1.67×10^{-5} *kg/kg* s^{-1}) corresponds to 1 *g/kg* freezing in 1 *min*.

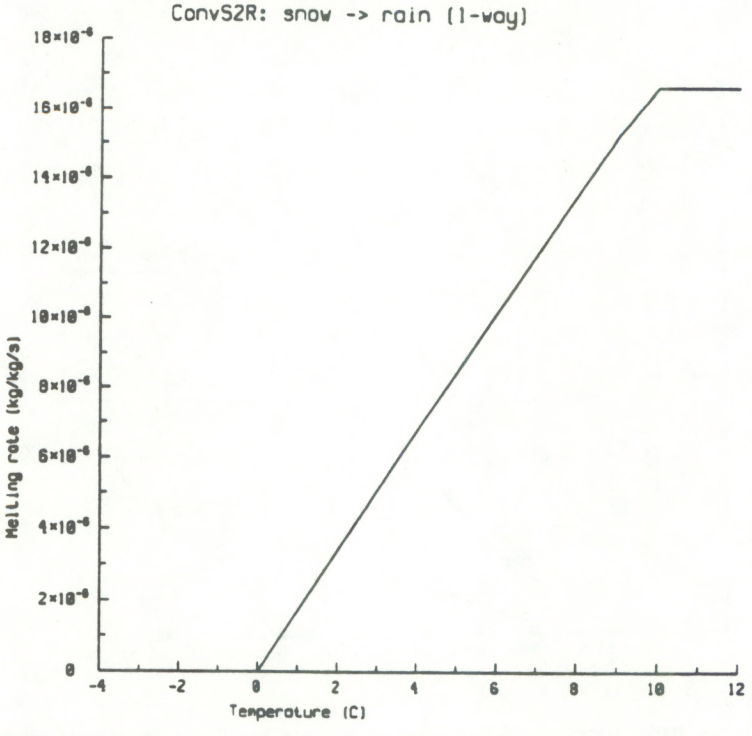

Figure 2b. Conversion function for snow melting into rain. The conversion rate parameter (1.67×10^{-5} *kg/kg* s^{-1}) corresponds to 1 *g/kg* melting in 1 *min*.

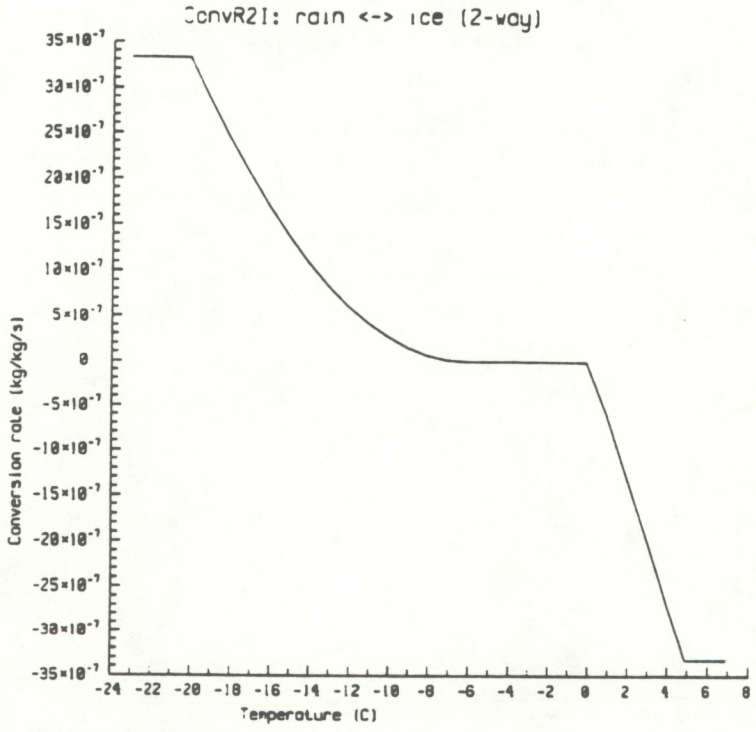

Figure 2c. Conversion function for rain freezing to ice and ice melting to rain. This function is identical to that shown in Figure 2a, but the rate parameter (0.33 x 10^{-5} *kg/kg* s^{-1}) is lower (slower).

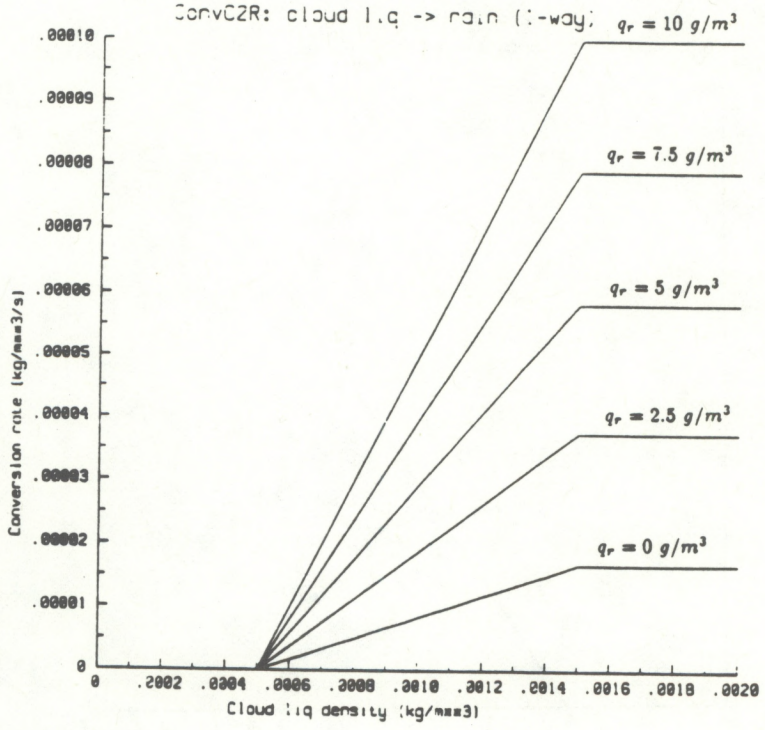

Figure 2d. Conversion function for cloud liquid accretion by rain, including autoconversion. The conversion rate parameter (1.67 x 10^{-5} $kg/m^3\ s^{-1}$) corresponds to 1 g/m^3 converted in 1 *min*.

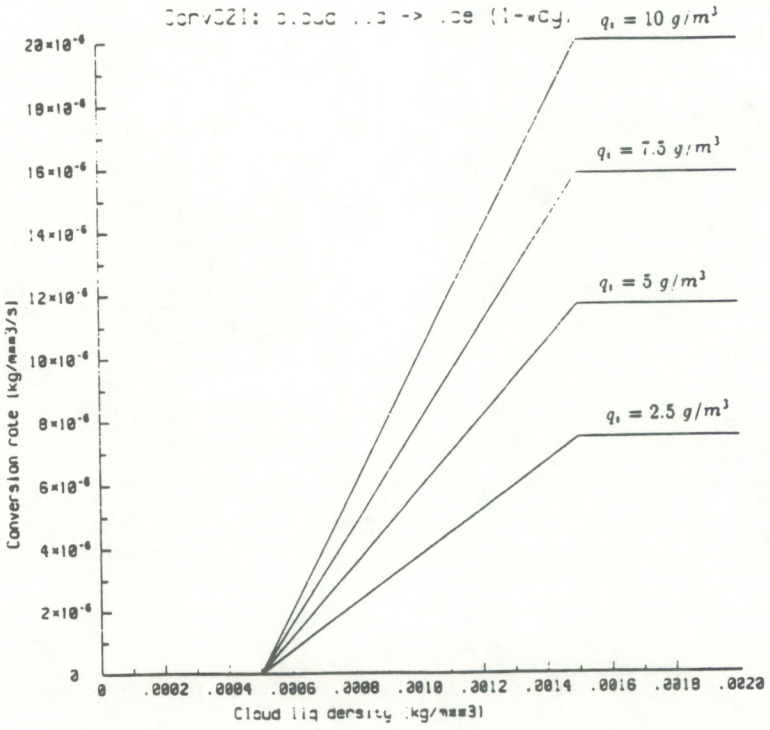

Figure 2e. Conversion function for cloud liquid accretion by ice. This is the same function as in Figure 2d, but the rate parameter (0.83 x 10^{-5} kg/m^3 s^{-1}) is lower (slower).

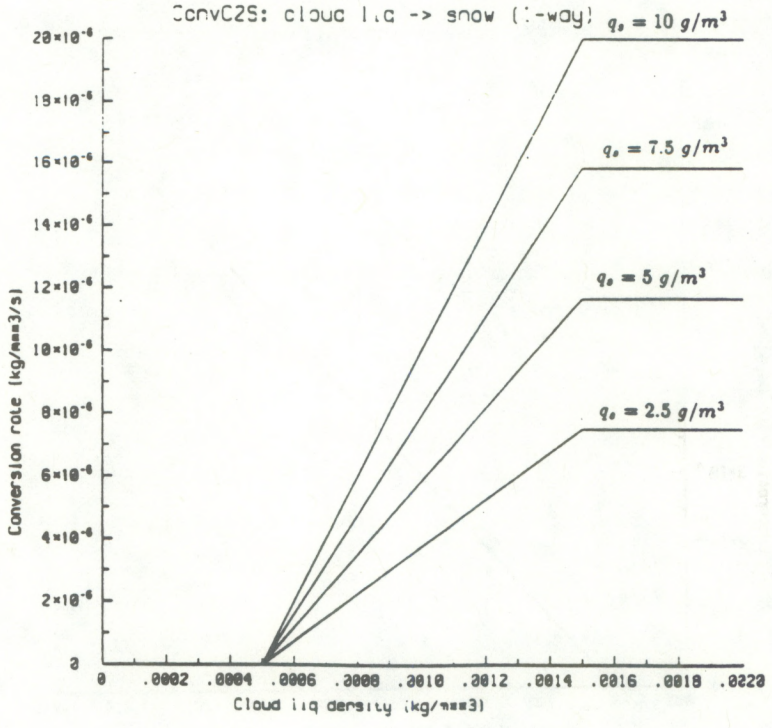

Figure 2f. Conversion function for cloud liquid accretion by snow. This is the same function as in Figure 2d, but the rate parameter (0.83 x 10^{-5} kg/m^3 s^{-1}) is lower (slower).

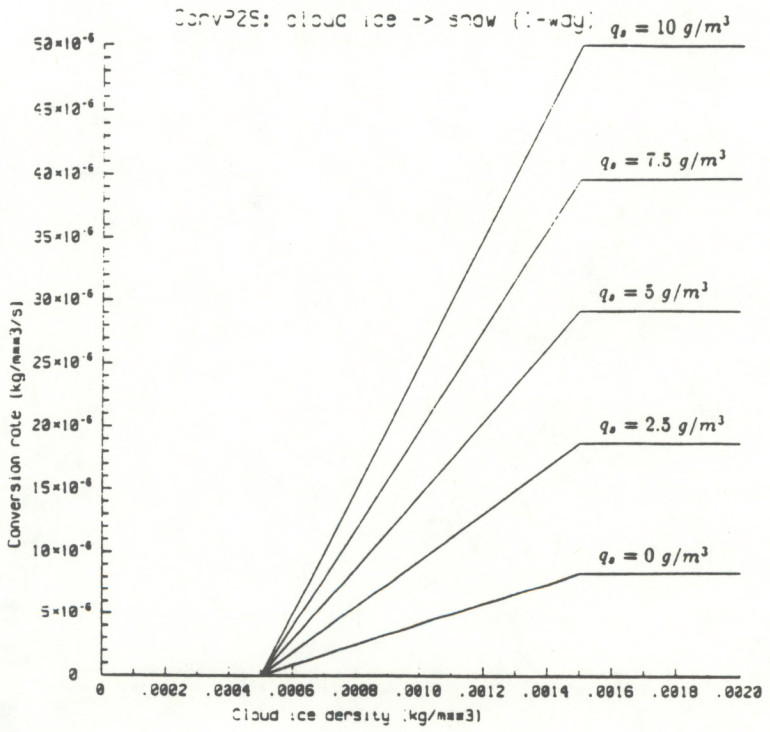

Figure 2g. Conversion function for cloud ice growing or collecting into snow, including autoconversion. This is the same function as in Figure 2d, but the rate parameter (0.83 x 10^{-5} kg/m^3 s^{-1})is lower (slower).

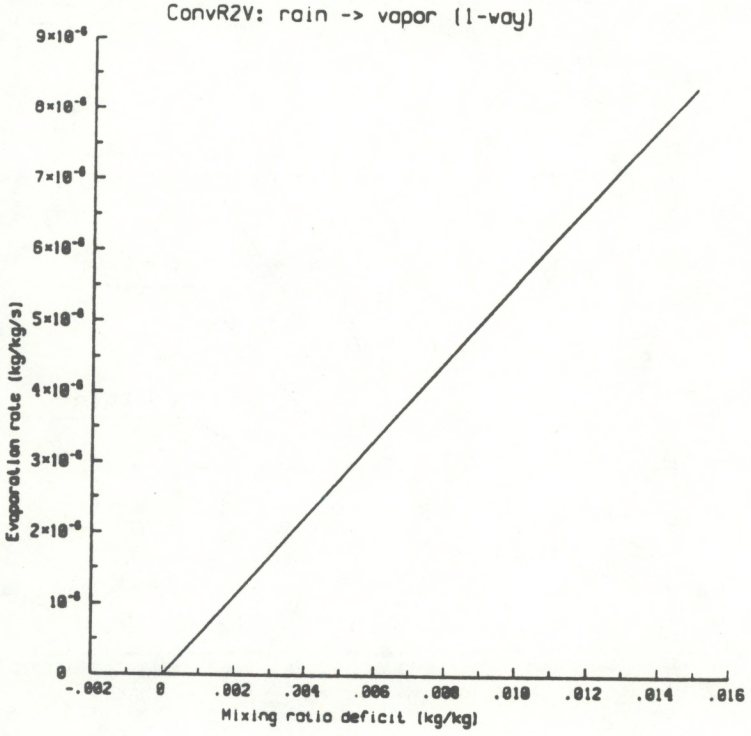

Figure 2h. Evaporation function for rain. The conversion rate parameter (0.83 x 10^{-5} kg/kg s^{-1}) corresponds to 1 g/kg evaporating in 2 min.

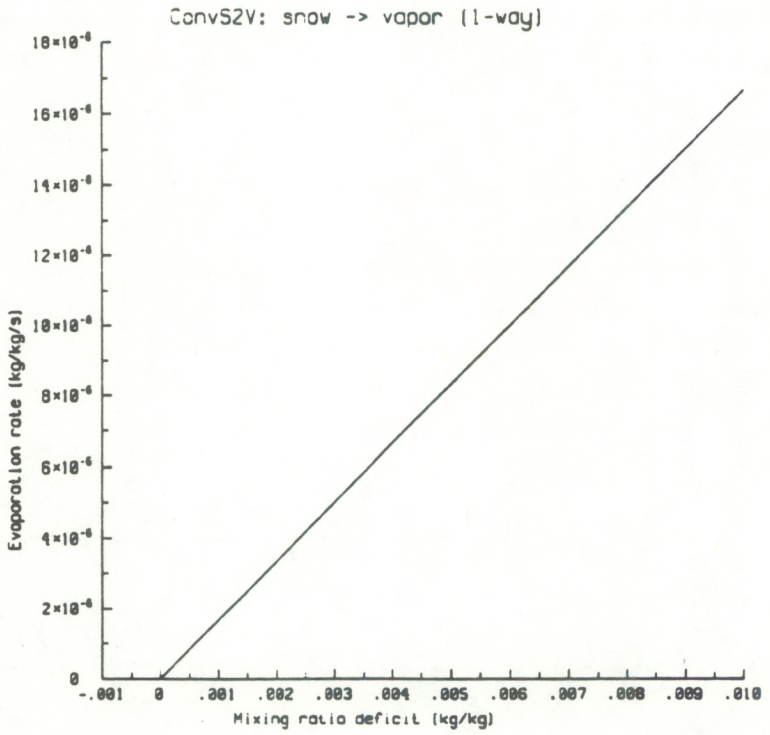

Figure 2i. Evaporation function for snow, which is identical to that for rain (Fig. 2h), but the conversion rate parameter (1.67×10^{-5} *kg/kg* s^{-1}) is higher (faster).

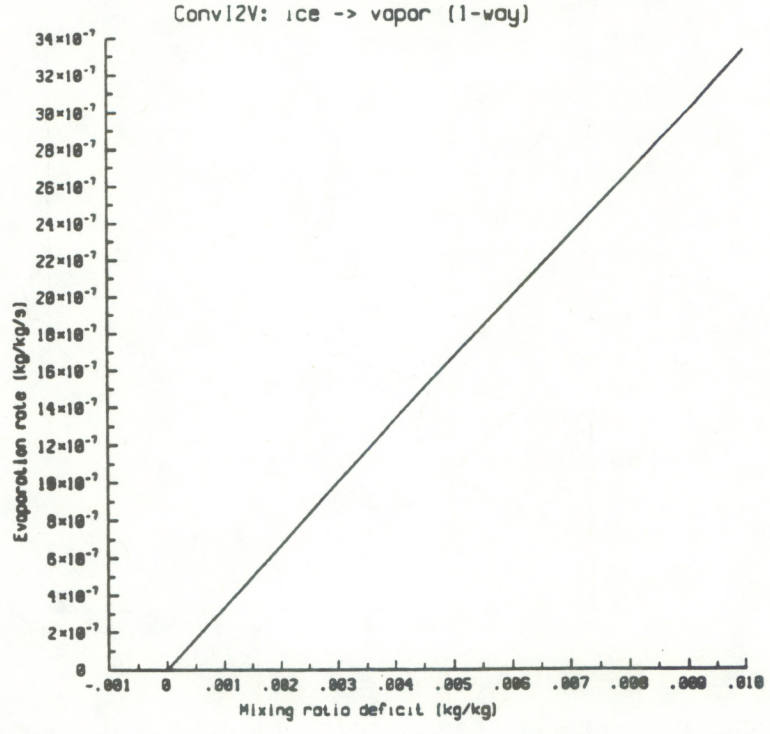

Figure 2j. Evaporation function for ice, which is identical to that for rain (Fig. 2h), but the conversion rate parameter (0.33×10^{-5} *kg/kg* s^{-1}) is lower (slower).

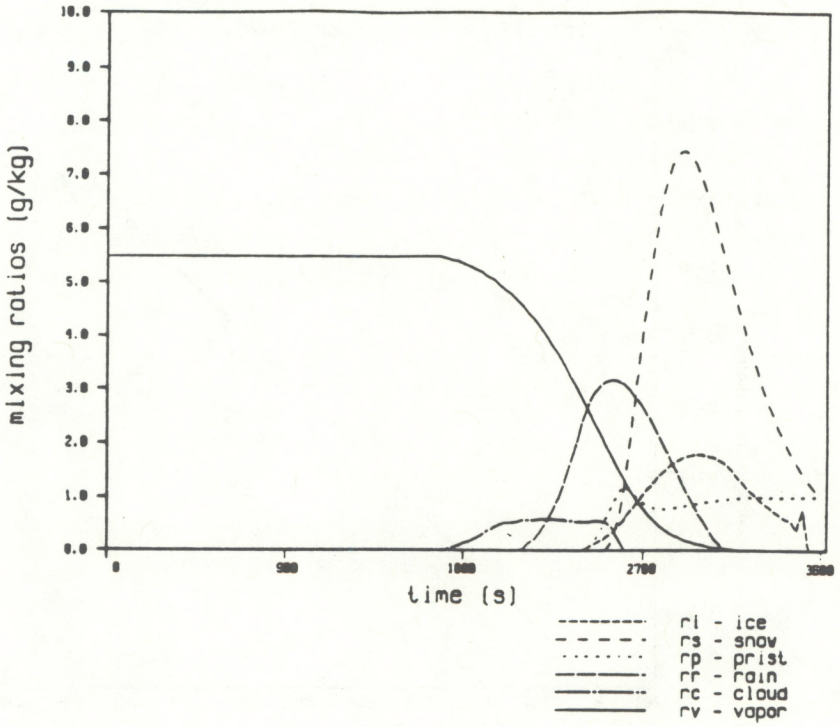

(a)

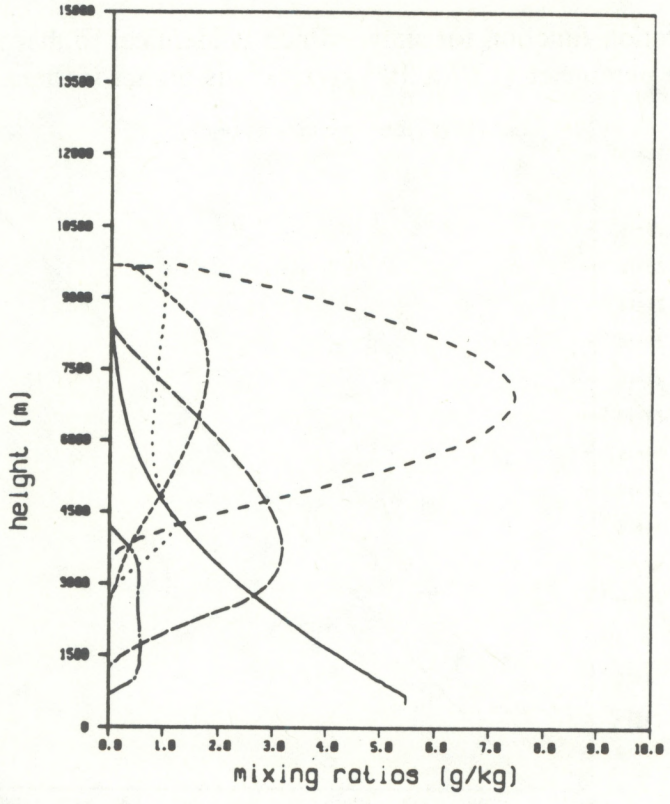

(b)

Figure 3. Condensate amounts in a parcel carried aloft by a thunderstorm. Progression is shown as a function of height (a) and time (b). The label "rp - prist" refers to pristine crystals, or cloud ice.

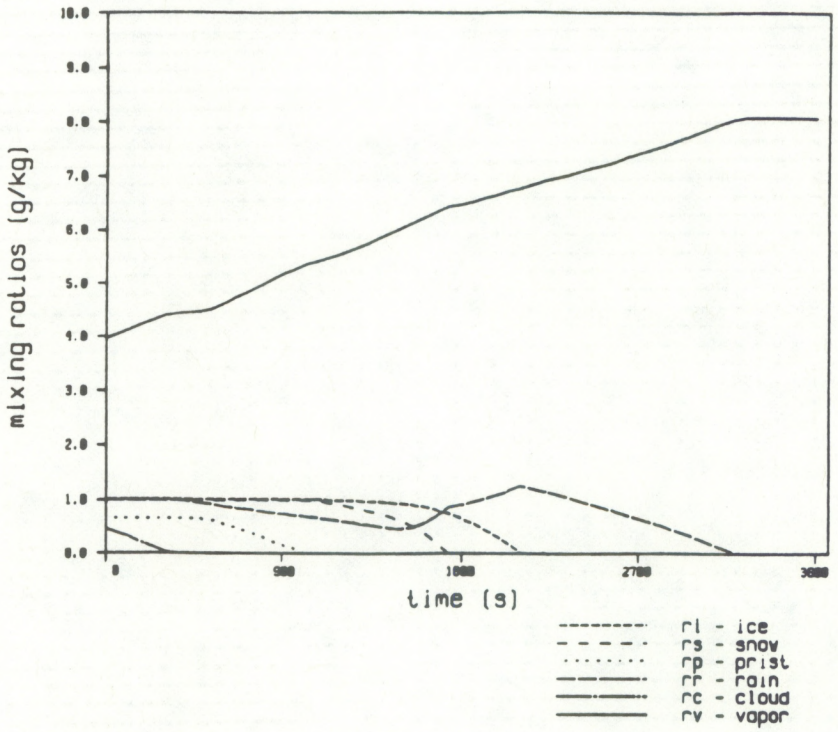

(a)

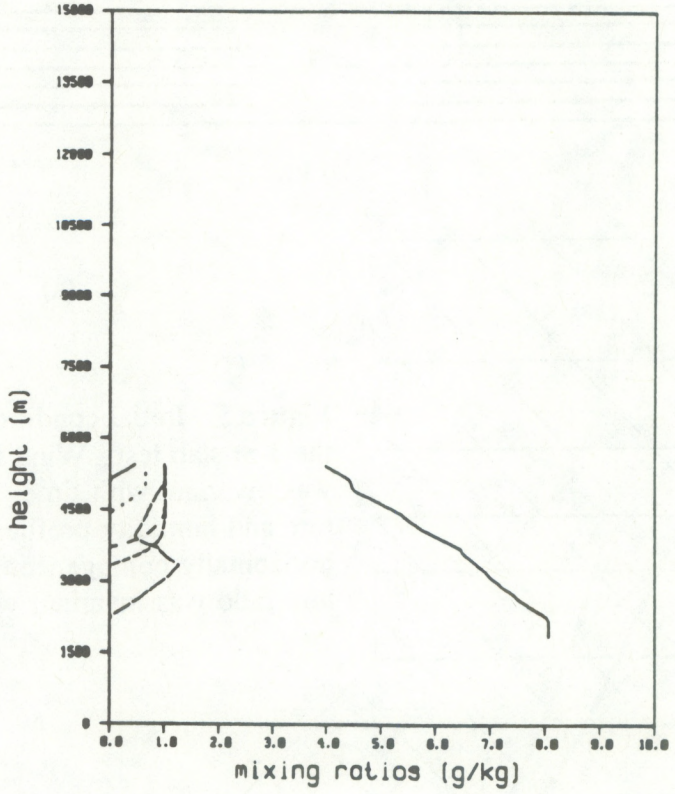

(b)

Figure 4. Condensate amounts in a slowly descending parcel. As in Figure 3.

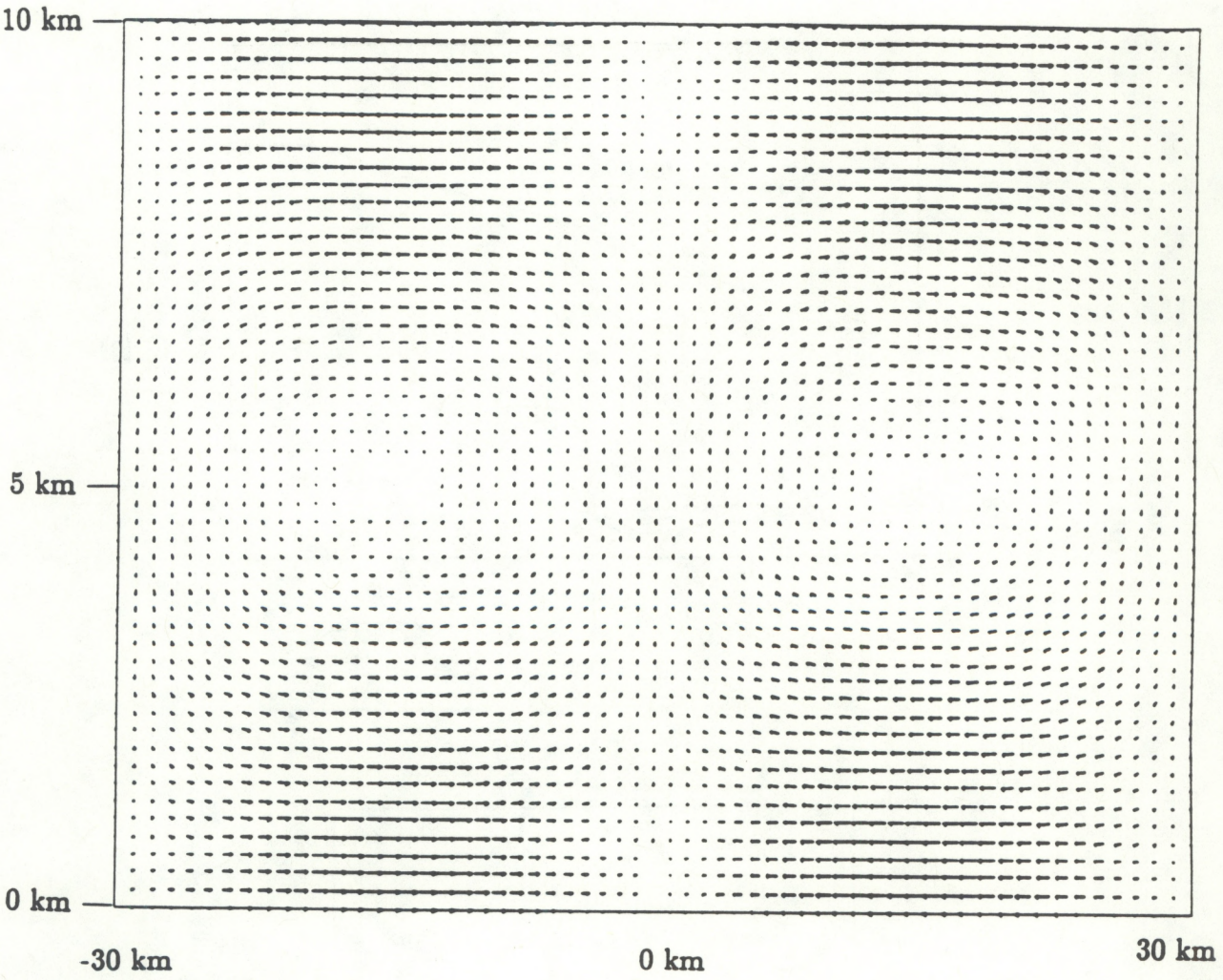

(a)

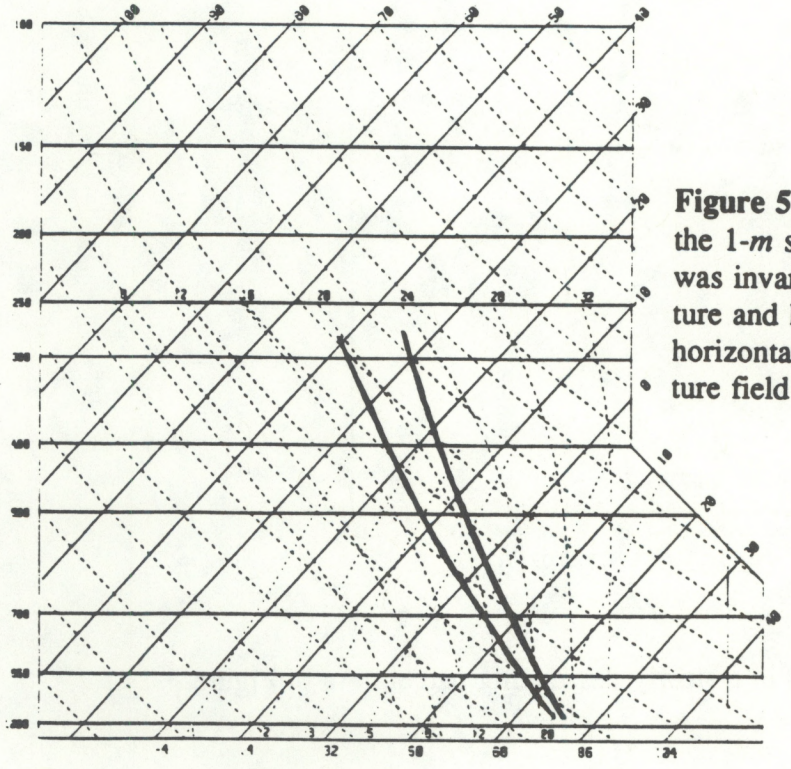

(b)

Figure 5. Initial conditions for the 1-*m* slab test. Wind field (a) was invariant with time. Temperature and humidity profiles (b) were horizontally homogeneous. Temperature field was invariant with time.

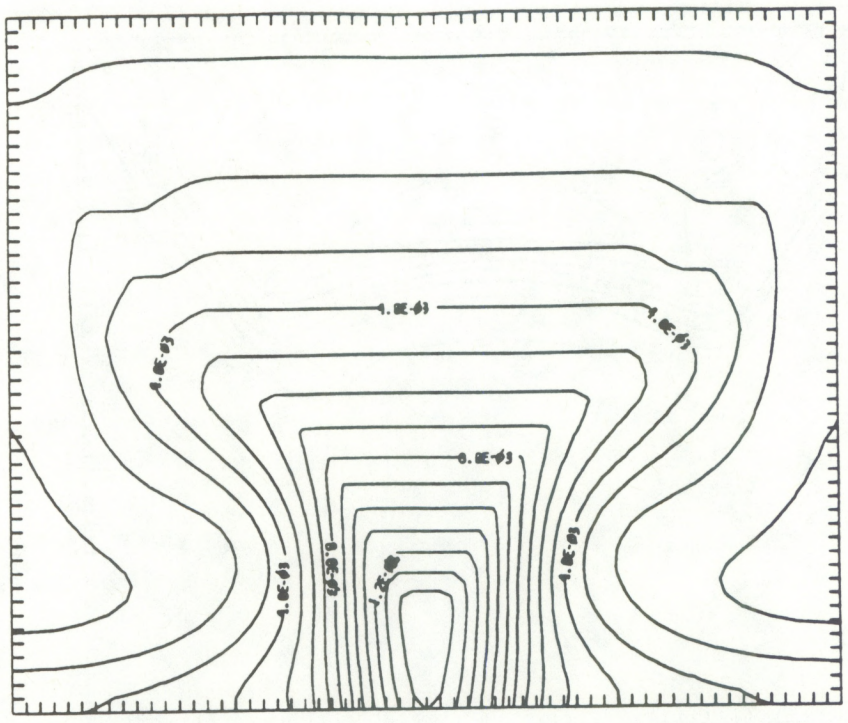

Figure 6a. Water vapor field in the slab model after 30 *min*. Contour increment is 1 *g/kg*.

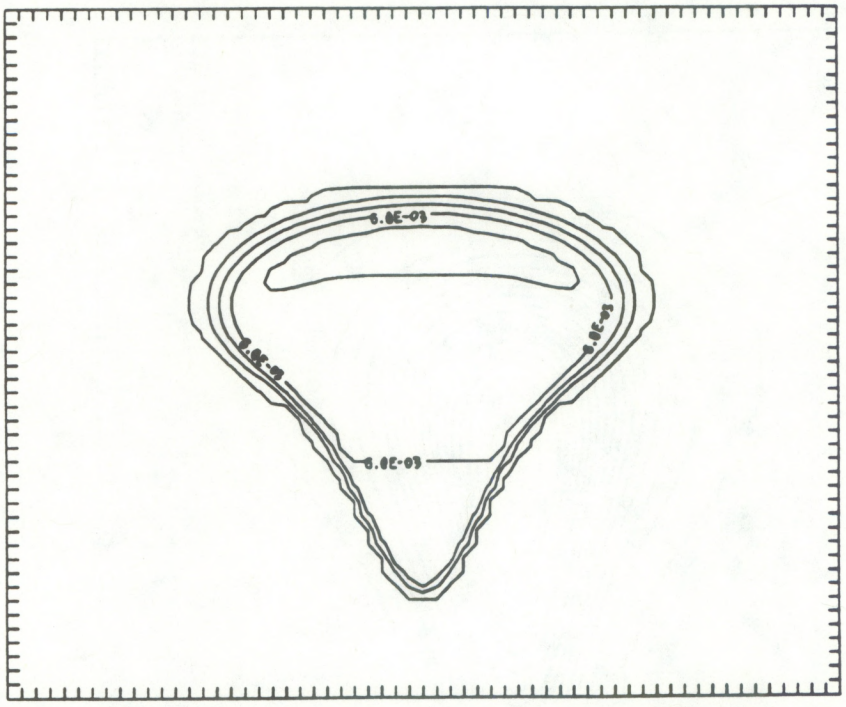

Figure 6b. Cloud liquid in the slab model after 30 *min*. Contour increment is .2 *g/kg*.

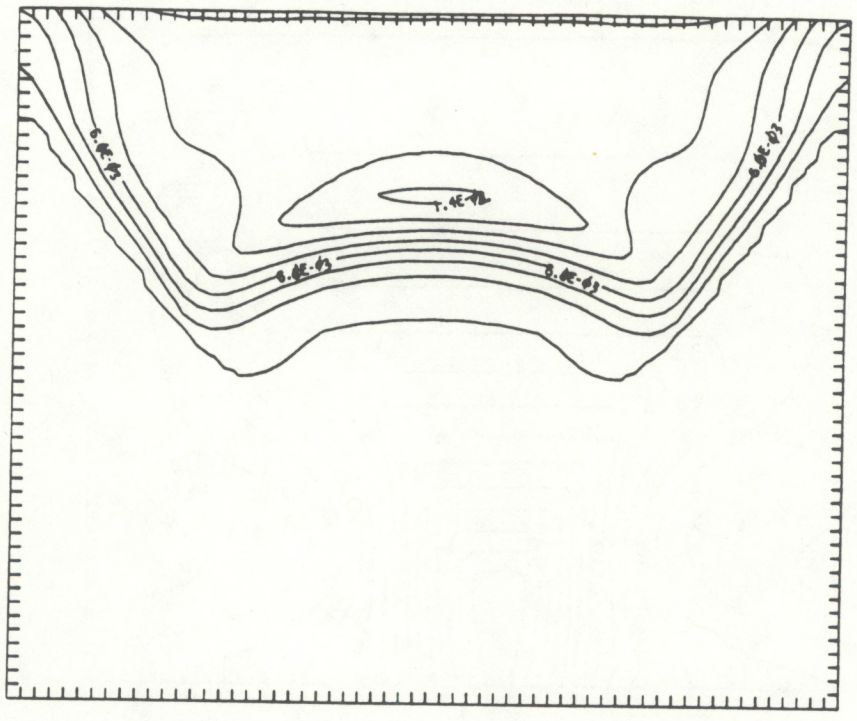

Figure 6c. Cloud ice in the slab model after 30 *min*. Contour increment is .2 *g/kg*.

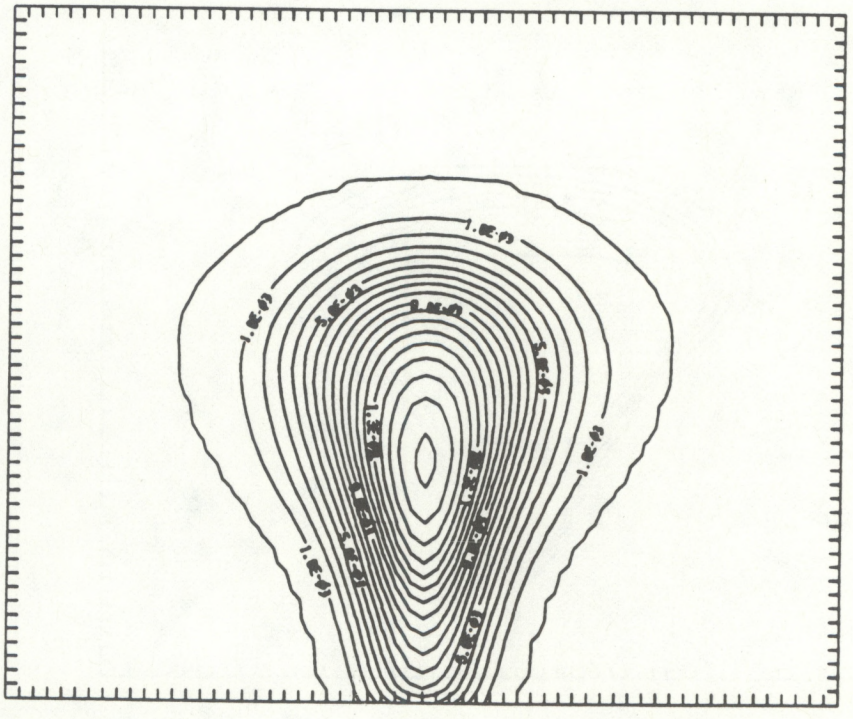

Figure 6d. Rain water in the slab model after 30 *min*. Contour increment is 1 *g/kg*.

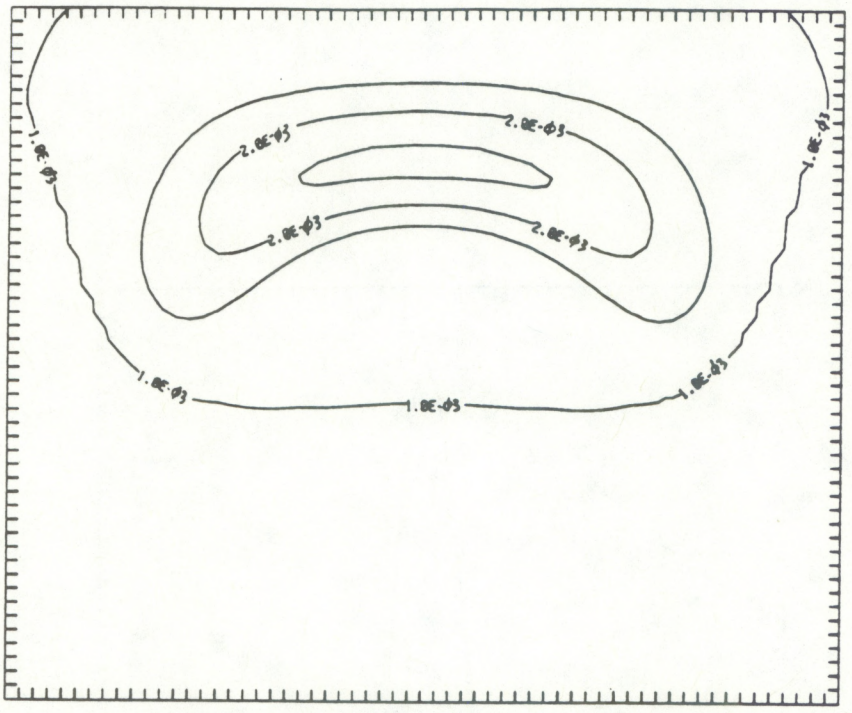

Figure 6e. Snow water in the slab model after 30 *min*. Contour increment is 1 *g/kg*.

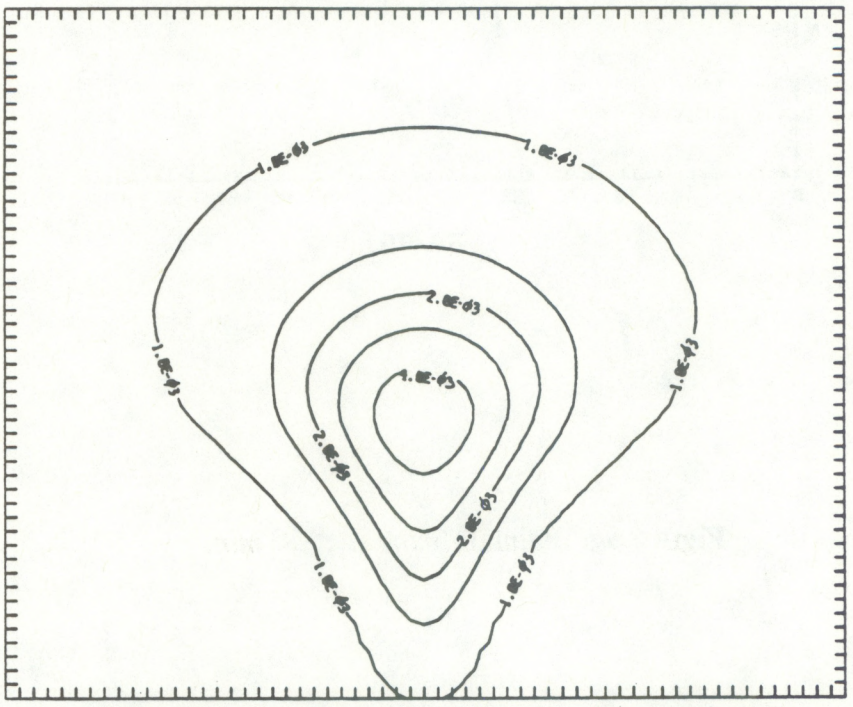

Figure 6f. Ice water in the slab model after 30 *min*. Contour increment is 1 *g/kg*.

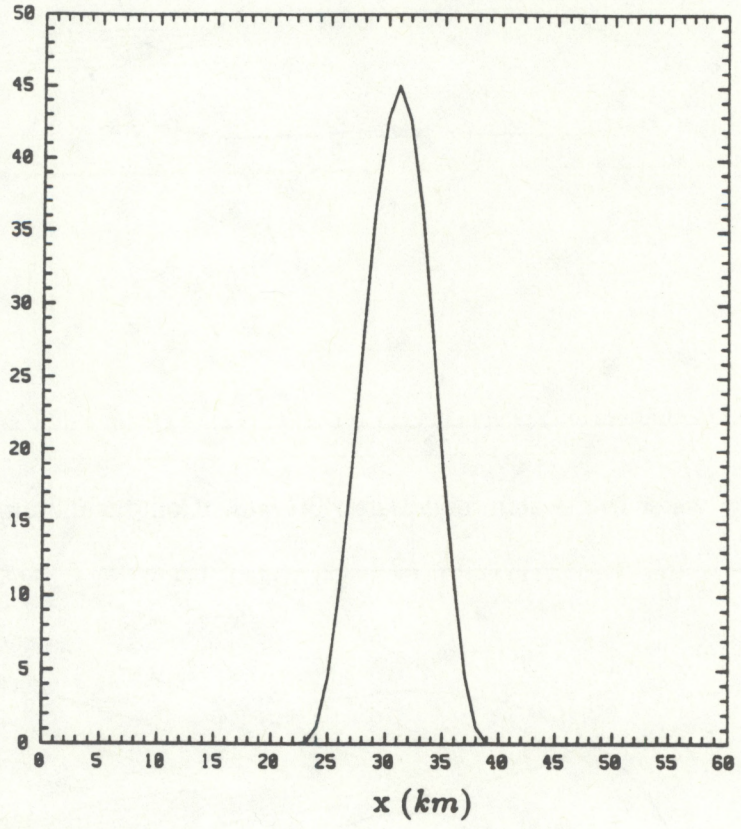

Figure 6g. Rainfall (*mm*) after 30 *min*.

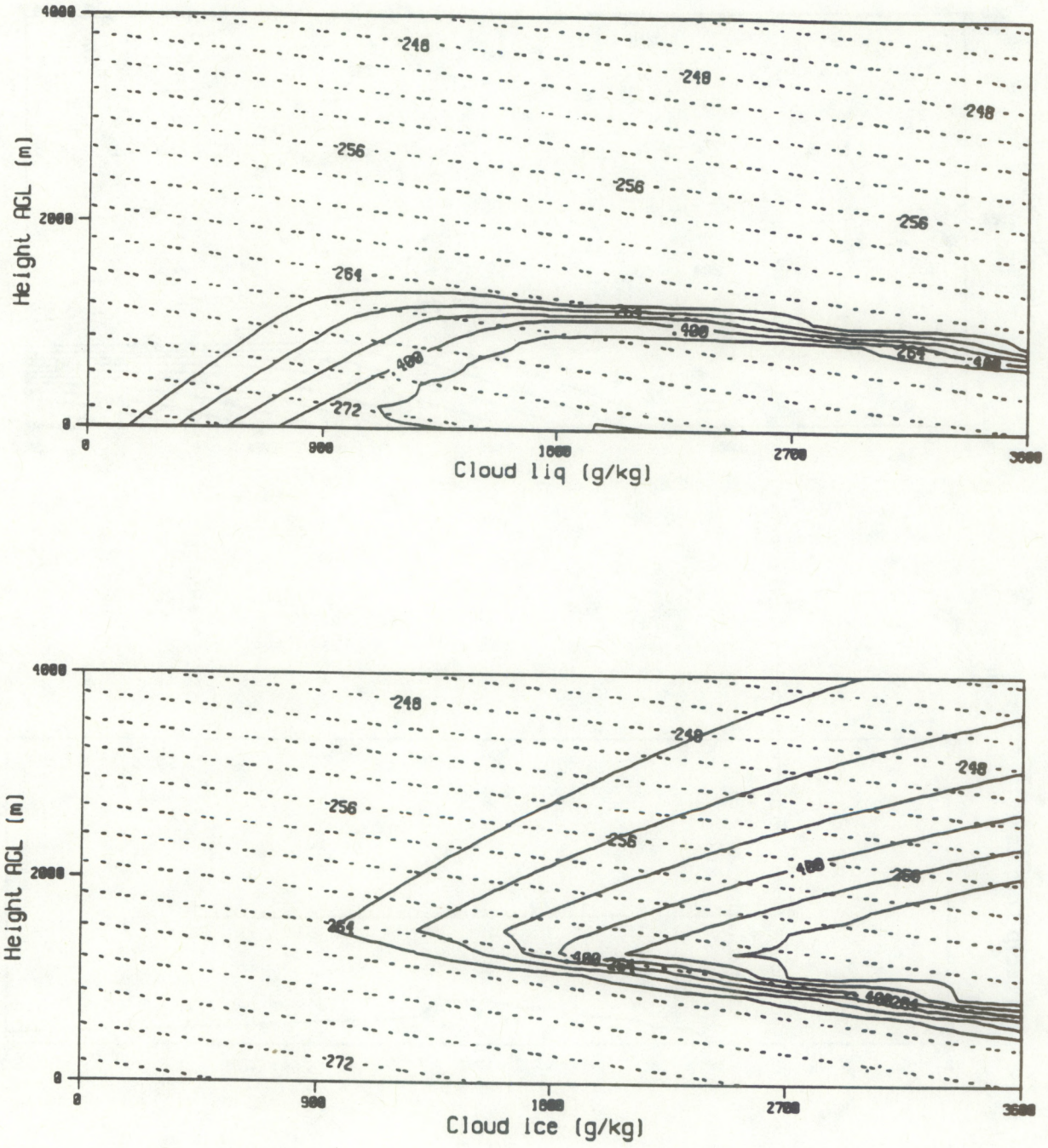

Figure 7a. Time series of cloud matter in the upslope-moving column simulation; liquid (above) and ice (below). Contour interval is 0.1 *g/kg*. The dashed sloping lines are isotherms (K).

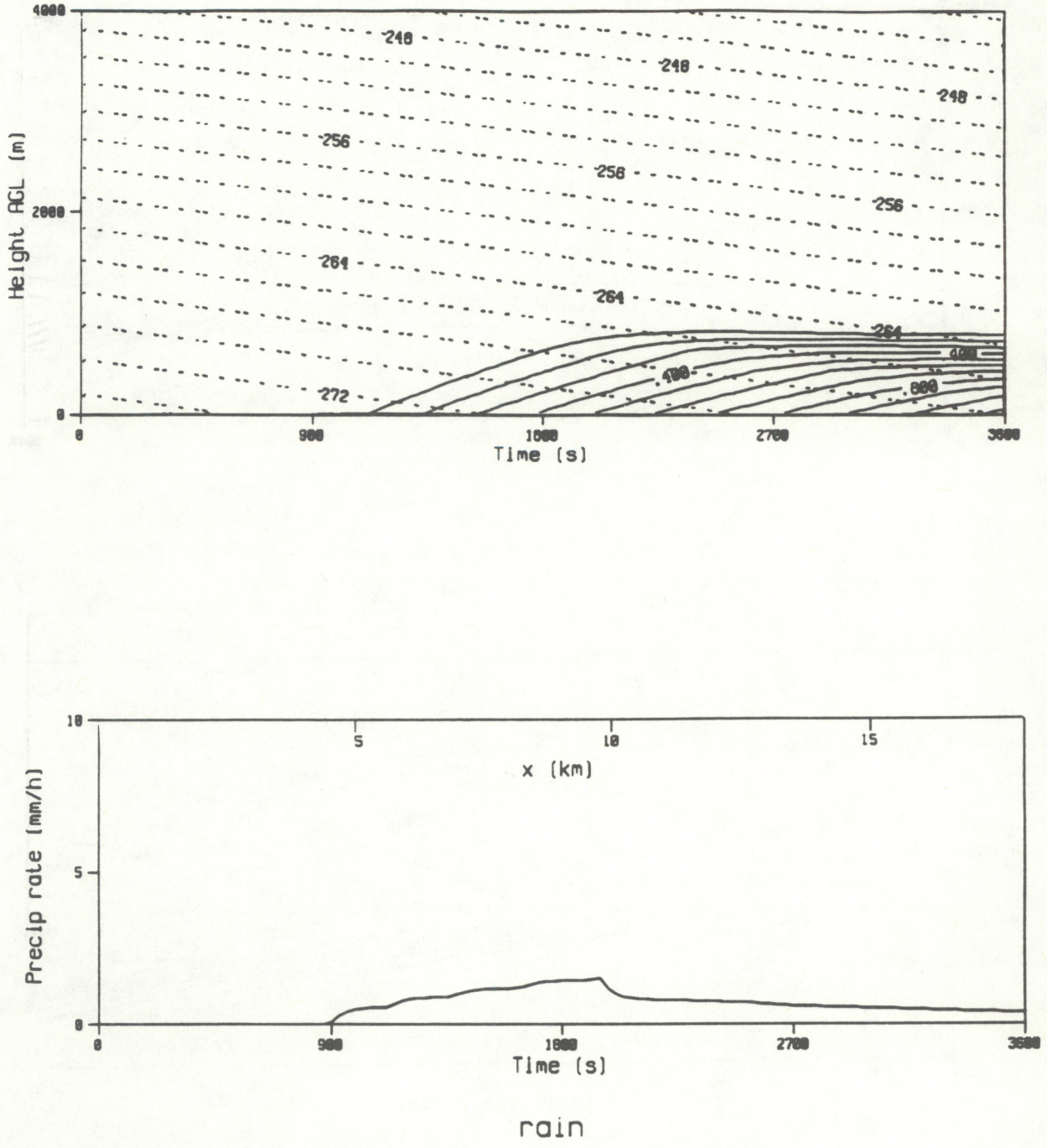

Figure 7b. Time series of rain content (above) and precipitation (below).

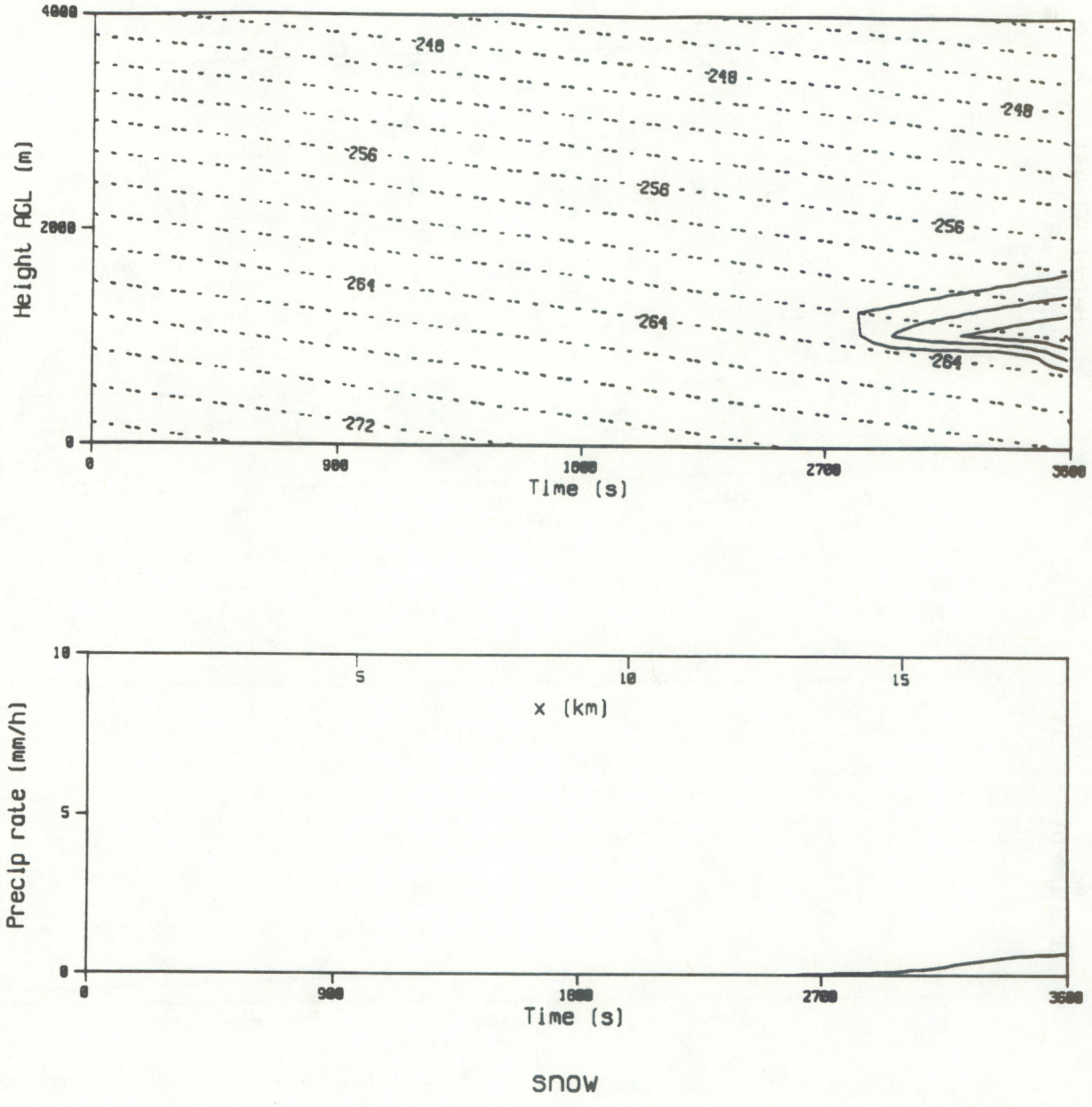

Figure 7c. As in Figure 7b, for snow.

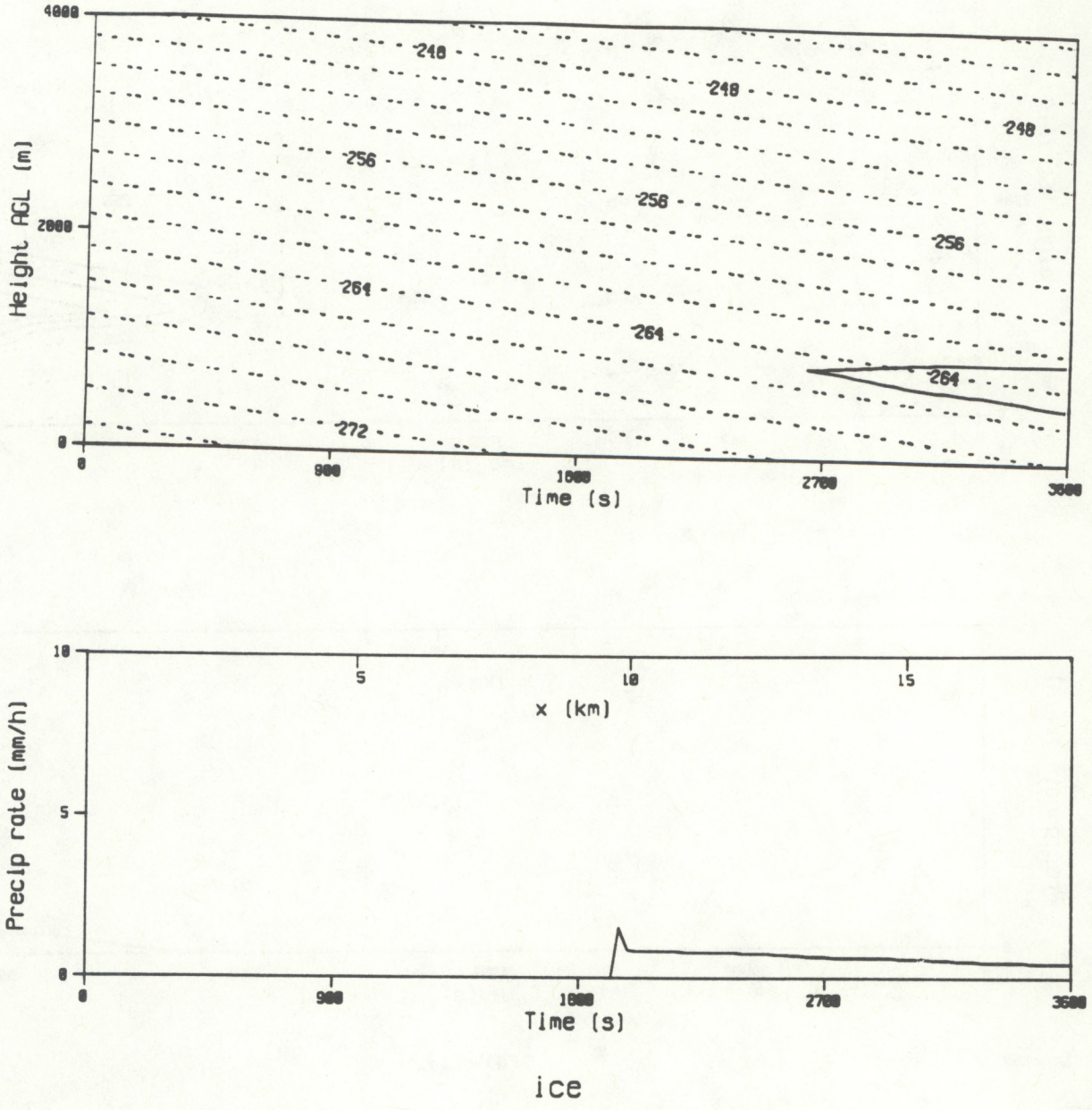

*U.S. GOVERNMENT PRINTING OFFICE: 1993-774-025/89026

Figure 7d. As in Figure 7b, for precipitating ice.